Remote Sensing of Environment 136 (2013) 47–55

Contents lists available at SciVerse ScienceDirect

Remote Sensing of Environment

journal homepage: www.elsevier.com/locate/rse

Toward the estimation of river discharge variations using MODIS data in ungauged basins

Angelica Tarpanelli [a,*], Luca Brocca [a], Teodosio Lacava [b], Florisa Melone [a], Tommaso Moramarco [a], Mariapia Faruolo [b], Nicola Pergola [b], Valerio Tramutoli [c]

[a] Research Institute for Geo-Hydrological Protection, National Research Council, Via Madonna Alta 126, 06128 Perugia, Italy
[b] Institute of Methodologies for Environmental Analysis, National Research Council, 85050 Tito Scalo (PZ), Italy
[c] University of Basilicata, Via dell'Ateneo Lucano 10, 85100 Potenza, Italy

ARTICLE INFO

Article history:
Received 5 September 2012
Received in revised form 16 April 2013
Accepted 20 April 2013
Available online xxxx

Keywords:
MODIS
Remote sensing
Discharge
Flow velocity
Po river

ABSTRACT

This study investigates the capability of the Moderate resolution Imaging Spectroradiometer (MODIS) to estimate river discharge, even for ungauged sites. Because of its frequent revisits (as little as every 3 h) and adequate spatial resolution (250 m), MODIS bands 1 and 2 have significant potential for mapping the extent of flooded areas and estimating river discharge even for medium-sized basins. Specifically, the different behaviour of water and land in the Near Infrared (NIR) portion of the electromagnetic spectrum is exploited by computing the ratio (C/M) of the MODIS channel 2 reflectance values between two pixels located within (M) and outside (C), but close to, the river. The values of C/M increase with the presence of water and, hence, with discharge. Moreover, in order to reduce the noise effects due to atmospheric contribution, an exponential smoothing filter is applied, thus obtaining C/M^*.

Time series of hourly mean flow velocity and discharge between 2005 and 2011 measured at four gauging stations located along the Po river (Northern Italy) are employed for testing the capability of C/M^* to estimate discharge/flow velocity. Specifically, the meanders and urban areas are considered the best locations for the position of the pixels M and C, respectively. Considering the optimal pixels, the agreement between C/M^* and discharge/flow velocity is fairly good with values in the range of 0.65–0.77. Additionally, the application to ungauged sites is tested by deriving a unique regional relationship between C/M^* and flow velocity valid for the whole Po river and providing only a slight deterioration of the performance. Finally, the sensitivity of the results to the selection of the C and M pixels is investigated by randomly changing their location. Also in this case, the agreement with *in situ* observations of velocity is fairly satisfactory ($r \sim 0.6$). The obtained results demonstrate the capability of MODIS to monitor discharge (and flow velocity). Therefore, its application for a larger number of sites worldwide will be the object of future studies.

1. Introduction

The important role of river discharge in the hydrological cycle is widely known, and its estimation is essential for both scientific and operational applications related to water resource management and flood risk prevention (Di Baldassarre & Uhlenbrook, 2011). Despite the awareness of the importance of river discharge information, many basins are still not monitored and, in recent decades, monitoring stations around the world have decreased (Calmant & Seyler, 2006; IAHS Ad Hoc Committee, 2001) thus constituting a global problem, above all in developing countries. The scarcity and sometimes absence of flow measurements along the natural channels contribute to making the discharge estimation difficult with negative impacts on water resource management.

In recent years, the availability of new and freely accessible data sources from satellite sensors is steadily increasing. Several studies have already addressed the possibility of estimating river discharge from space, demonstrating their feasibility and great potential for difficult-to-monitor river sites (Alsdorf et al., 2007; Birkinshaw et al., 2010; Bjerklie et al., 2003; Faruolo et al., 2009; Horritt et al., 2001; Neal et al., 2009; Smith & Pavelsky, 2008; Smith et al., 1996; Tarpanelli et al., 2011; Temimi et al., 2007). As discharge cannot be measured directly from space, Bjerklie et al. (2003) inferred it by using remotely sensed hydraulic variables (water-surface width, surface velocity and stage). In this way, different quantities can be measured separately through remote sensing and used, successively, for discharge estimation.

For very large river basins (>10,000 km^2), the use of microwave sensors and radar altimeters have proven to be very useful tools to integrate or even increase discharge monitoring (Birkinshaw et al., 2010; Temimi et al., 2007). For smaller basins (<10,000 km^2), Synthetic Aperture Radars (SARs) are usually employed for the indirect

* Corresponding author. Tel.: +39 0755014426.
E-mail address: a.tarpanelli@irpi.cnr.it (A. Tarpanelli).

0034-4257/$ – see front matter © 2013 Elsevier Inc. All rights reserved.
http://dx.doi.org/10.1016/j.rse.2013.04.010

estimation of water elevation (Matgen et al., 2011) but their low temporal resolution (around 30 days) might be considered insufficient for those rivers characterized by high temporal variability of discharge, for which readily available discharge estimates are required.

Passive microwave sensors have frequently been used for discharge estimation. For example, Advanced Microwave Scanning Radiometer for the Earth Observing System (AMSR-E) data has been used by Temimi et al. (2007) to monitor streamflow in the Mackenzie River basin in Canada, and by Temimi et al. (2011) for flood and river discharge monitoring during the 2008 flood in Iowa. Another noteworthy example is furnished by Brakenridge et al. (2007) that used AMSR-E data at 37 Ghz to globally infer river discharge. In particular, their approach is based on the ratio between the brightness temperature measured for a pixel unaffected by the river and a pixel centred over the river itself, respectively. This procedure has been implemented world-wide within the "Global Flood Detection System" (http://old.gdacs.org/flooddetection/overview.aspx) for more than 10,000 monitoring sites with the target of flood detection also for ungauged and inaccessible rivers from space. On the other hand, Brakenridge and Anderson (2006) demonstrated that the Moderate resolution Imaging Spectroradiometer (MODIS) sensor can be also used for operational hydrological applications, including not only flood detection and characterization but also discharge estimation. They reported only a single preliminary example in which the discharge is estimated by MODIS considering a very short time series (about 30 data). It's worth noting that the remote sensing signal is affected by the surface flow area changes and the discharge estimation can take place only using a method of calibration. Other studies have investigated the use of MODIS data for discharge estimation (Weissling & Xie, 2008). For example, Weissling and Xie (2009) used MODIS-derived indices of biophysical states along with rainfall data in a statistical prediction model of streamflow. However, in these studies, the mean 8-day (or 16-day) discharge has been estimated, but is of little interest for hydrological applications related to the flood event.

Based on the above insights, we presented a study in which, to the best of our knowledge, for the first time a long time series of daily MODIS data is applied to discharge estimation, even for ungauged river sites. Specifically, the methodology developed by Brakenridge and Anderson (2006) and Brakenridge et al. (2005, 2007) is applied to four river sites along the Po river by using an extended time period covering 7 years from 2005 to 2011. Hourly observation of flow velocity and river discharge are employed to test the reliability of MODIS data. Moreover, through an in-depth investigation into the relationship between MODIS-derived discharge and *in situ* observations, an attempt is also made to regionalize this relationship for its application in ungauged sites.

2. Study area

The Po River is located in the centre of a large flat alluvial plain, the Pianura Padana (Po Valley), which is a very important agricultural region and industrial heart of Northern Italy. For this study four gauged river sites along the river, which continuously monitor the water level, are used: Piacenza (basin area equal to 42,030 km^2), Cremona (50,726 km^2), Borgoforte (62,450 km^2) and Pontelagoscuro (70,091 km^2) (Fig. 1). The geometric characteristics of the four analysed gauging stations (see Table 1) were deduced by a ground survey conducted by the Interregional Agency of the River Po in 2005. The riverbed consists of a stable main channel with a width varying from 200 to 300 m and two lateral banks (the overall width varies from 400 to 4 km) confined by two artificial levees. The river depth ranges from about 10 to 18 m.

Table 1
Characteristics of the gauging stations of the Po River: basin area (A_b), river width (w), river depth (d), maximum discharge (Q_{max}), minimum discharge (Q_{min}), mean discharge (Q_m).

Gauged station	A_b (km^2)	w (m)	d (m)	Q_{max} (m^{3}s^{-1})	Q_{min} (m^{3}s^{-1})	Q_m (m^{3}s^{-1})
Piacenza	42,030	213	18.01	12,800	125	958
Cremona	50,726	285	12.86	13,750	200	1115
Borgoforte	62,450	274	10.47	12,047	209	1373
Pontelagoscuro	70,091	302	17.24	10,300	156	1501

The data of water level, h, for all the stations are recorded with a time interval of 30 min. In particular, seven years of data, from January 2005 to December 2011, are selected. It must be noted that the knowledge of river discharge, Q, at the selected gauging stations is derived by a rating curve obtained by the observed data of water level and velocity measurements, v, occasionally collected for different discharge conditions; for each gauged site the h–v pairs is greater than 22 thus allowing to obtain reliable rating curves. As regards the flow regime, the values of maximum, mean and maximum discharge are reported in Table 1 for the four gauging stations.

Besides discharge, which is fundamental for water resource management, mean flow velocity data are also used as benchmarks in this study. These data may be more suitable for the scope of this work taking the local conditions of the river geometry into account. The mean flow velocity, v, considered in the analysis is simply computed as the ratio between Q and the river section area, A, i.e. $v = Q/A$.

3. MODIS dataset

MODIS is one of the sensors aboard the EOS Terra and Aqua satellites. MODIS has been widely used for monitoring several terrestrial, atmospheric, and ocean phenomena thanks to its high spectral resolution of 36 bands ranging in wavelength from 0.4 μm to 14.4 μm, its moderate spatial resolution (2 channels at 250 m, 5 at 500 m and 29 at 1 km), its good temporal resolution of 1–2 days with sometimes at mid-latitude two passes in daytime (3 h apart each other), and its multi-year operational continuity flying on (Terra since 1999 and on Aqua since 2002) (Friedl et al., 2010).

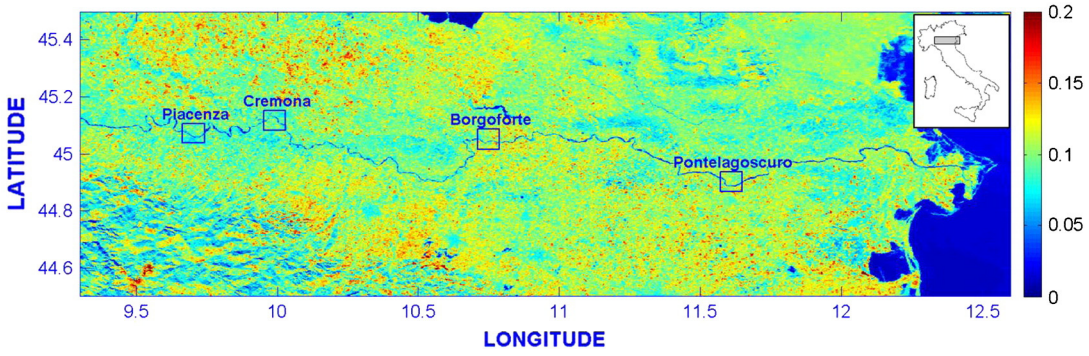

Fig. 1. Location of the study sites on the AQUA-MODIS image of 13th February 2005 at 12:20 GMT (Channel 2 reflectance shown in false-color).

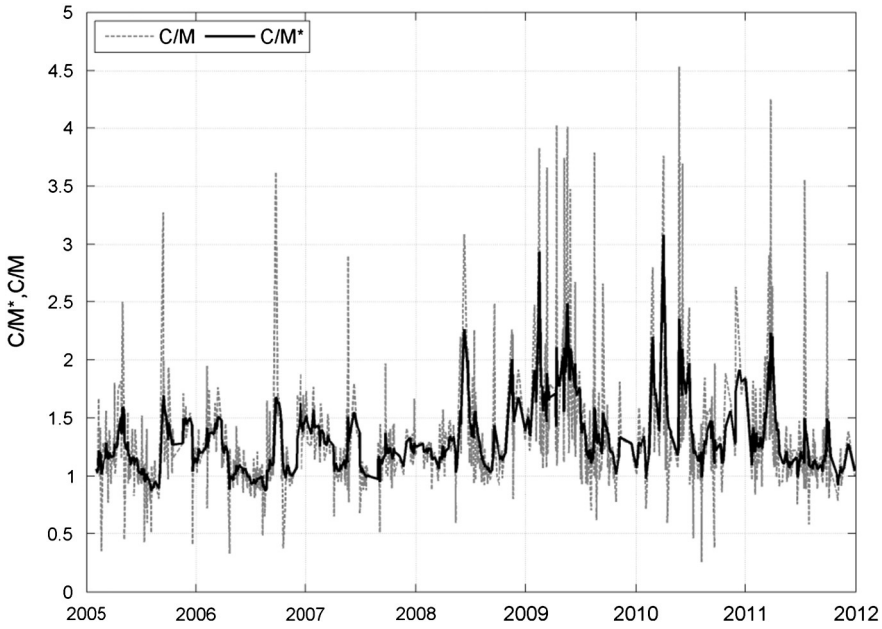

Fig. 2. Temporal pattern of C/M and C/M^* (filtered values) time series for Pontelagoscuro gauged site.

For this study, MODIS channel 1 (0.620–0.670 μm — Red) and channel 2 (0.841–0.876 μm –Near Infrared) data were extracted from MODIS level 1b (MOD02QKM and MYD02QKM) data sets, acquired by the sensor aboard Aqua satellite. The data from Terra satellite were not analysed because they performed worse than Aqua probably due to the influence of fog on the morning passage of this satellite (i.e., 9:30–11:30 GMT), especially during winter. In particular, all the images acquired in the period 2005–2011 over Northern Italy (local time of passage ranges from 12:30 to 14:30 GMT) were first processed obtaining surface reflectance values (R_1 and R_2). Successively, for each image, a sub-scene sized 1320×400 pixels centred on the Po basin was extracted, obtaining globally 4764 sub-scenes (2382 for R_1 and 2382 for R_2), almost one per day. An example of the sub-scene of February 13, 2005 at 12:20 GMT is shown in Fig. 1 along with the location of the four gauged sites used here. It should be stressed that a possible source of noise in our historical series might be related to MODIS Aqua data geolocation accuracy (not better than ± 50 m). Nevertheless, the exponentially smoothing filter used in this work (see next section) allows us to reduce its impact on the analysed time series.

4. Methodology

The approach proposed by Brakenridge and Anderson (2006) and Brakenridge et al. (2005, 2007), was adopted here. MODIS channel 2 data, acquired in the Near Infrared (NIR) portion of the electromagnetic spectrum with a spatial resolution of 250 m, were used. Specifically, the different spectral behaviour of water and land at these wavelengths was exploited. In the NIR region reflectance values of common land cover types (such as bare or vegetated soils), have extremely higher values than water pixels. In any given area, during a flood event, water surface increases causing a decrease in the NIR reflectance value of the area detected by the satellite. A possible slight increase in these values due to the presence of suspended sediment is in any case smoothed out by combining the signals coming from the different sub-pixel elements (i.e., turbid water, soil, vegetation) which make up the area observed by satellite. However, reflectance measurements are affected by significant noise induced by atmospheric factors. Following Brakenridge et al. (2007) and considering these constant noises over a large area (about 50 km^2), their contribution can be minimized by comparing two signals, one for land

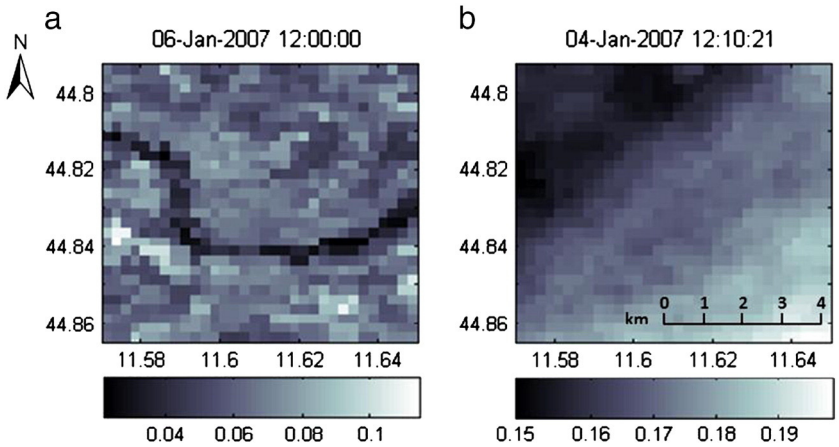

Fig. 3. Channel 2 MODIS reflectance image surrounding the Pontelagoscuro site. Examples of images without (a) and with (b) cloud cover.

Table 2
Coefficients of correlation, *r*, between the hydrological variables *Q*, *v* and the ratio unfiltered *C*/*M* and filtered C/M^*, between the reflectance value of the wet pixel *M* and one of the dry pixel *C*. *r* is considered for the *C*/*M* calculated considering the optimized location for pixels *M* and *C*. The number of images selected for the analysis is also reported.

Gauged station	Number of images	*C*/*M*		C/M^*	
		Q	*v*	*Q*	*v*
Piacenza	864	0.51	0.51	0.65	0.67
Cremona	798	0.60	0.61	0.75	0.77
Borgoforte	1103	0.49	0.48	0.66	0.68
Pontelagoscuro	921	0.49	0.48	0.73	0.74

and one for water. Specifically, the ratio between the surface reflectance of a land pixel, named *C* (calibration), located near the river in an area free of surface water even during high flooding, and of a water pixel, named *M* (measurement), located within the river with the permanent presence of water, was calculated. This ratio, *C*/*M*, is a sensitive and consistent measurement of surface water. In fact, due to the variations of water volume during flood events, the reflectance of the wet pixel should decrease, while that of the dry pixel should remain fairly constant. Consequently, in case of flooding the *C*/*M* ratio should be sensitive to the increase of wet pixels and, hence, discharge.

We note that, for many applications (Brakenridge et al., 2012), the discharge (or water level) variations may be sufficient information. However, in this study the quantitative estimation of discharge is addressed since, mainly for ungauged basins, this could be of particular interest. In fact, the knowledge of distributed discharge information can be very beneficial in transboundary basins where it can be used to solve conflicting management objectives, for which remote sensing data would represent a unique source of data.

Moreover, differing from previous studies (Brakenridge et al., 2005; De Groeve & Riva, 2009), a single pixel was used here instead of considering the average over a box of several pixels. In fact, several attempts were also made by using boxes of 2×2 and 3×3 pixels but, on average, the results (not shown for brevity) are worse than the one obtained here. Moreover, for smaller rivers, if compared to those usually investigated through remote sensing data, we believe that by using a single pixel the actual variability of the reflectance values is better preserved.

From each MODIS image, a box centered on each investigated gauging station was selected for which the following analyses were carried out. Before extracting the *C*/*M* ratios, a quality check of the images was carried out. Firstly, a simple fixed threshold on R_1 channel was employed to exclude pixels affected by snow and cloud cover. Then, a visual screening was carried out to identify and discard the images still affected by clouds. The quality-checked images were used for the computation of the *C*/*M* ratio of each pixel surrounding the gauged sites.

Even though the *C*/*M* ratio is of support to minimize the noises of the surface reflectance values, *C*/*M* varies rapidly in time and appears quite erratic (see for example Fig. 2). To reduce the effects of short term and observation noises, also related to the conditions of illumination (e.g. sun/sensor position), an exponentially smoothing filter (Albergel et al., 2008; Wagner et al., 1999) was applied to the data stream. Such a filter uses a single tuning parameter (the characteristic time length, *T*) and continually calculates a smoothed value given by a weighted average of recent observations giving less weight to older data. The recursive formulation of the method relies on (Albergel et al., 2008):

$$C/M^*_{t_{n+1}} = C/M^*_{t_n} + K_{t_{n+1}}\left[C/M_{t_{n+1}} - C/M^*_{t_n}\right] \quad (1)$$

where $C/M_{t_{n+1}}$ is the value of the ratio at time t_{n+1} and $C/M^*_{t_n}$ is the filtered value at previous time, t_n. The gain *K* ranges between 0 and 1 and is given by:

$$K_{t_{n+1}} = \frac{K_{t_n}}{K_{t_n} + e^{-\left(\frac{t_{n+1}-t_n}{T}\right)}} \quad (2)$$

For the initialization of this filter, K_{t_1} and $C/M^*_{t_1}$ were set to 1 and C/M_{t_1}, respectively. Hereafter, the time dependence of $C/M^*_{t_n}$ was dropped yielding to C/M^* (Fig. 2).

Finally, the C/M^* ratio was compared with the *Q*, *v* time series extracted by *in situ* sensors in correspondence of the dates of the satellite overpasses. The agreements between C/M^* and *Q* or *v* time series have been assessed in terms of coefficient of correlation, *r*, root mean square error, *RMSE*, Nash–Sutcliffe efficiency, *NS* (Nash & Sutcliffe, 1970), mean absolute error, MAE and 10th, 50th and 90th percentiles of the absolute error distribution.

In summary, for each investigated gauging station the following processing steps were carried out:

1) from each MODIS image, a box of size $J \times K$ centered on the investigated gauging station was selected;
2) pixels affected by cloud cover and/or snow were identified by using a fixed threshold on R_1 ($R_1 > 0.2$), confirmed by visual inspection, and discarded;
3) the mean daily discharge, *Q*, and mean daily flow velocity, *v*, measured at the gauging station and corresponding to the acquisition dates of the satellite sensor overpasses were selected;
4) for each pixel *i* ($i = 1, 2, \ldots, J \times K$), the matrix $X\,[N, J \times K - 1]$ of the *C*/*M* time series was calculated by assuming the pixel *i* as *C* and the remaining ones as *M*, *N* represents the number of available imagery. In particular, *X* is formed by $J \times K - 1$ columns, each one representing the *C*/*M* time series of length *N*. Finally, $(J \times K) \times (J \times K - 1)$ *C*/*M* time series of length *N* were obtained.
5) the smoothing exponential filter was applied to the *C*/*M* time series, thus obtaining C/M^* time series, and the *C* and *M* optimal location as well as the optimal *T*-value were identified by using the velocity observations, *v*, as benchmark.

Finally, with the aim to address the procedure for ungauged river sites, a preliminary analysis based on the random selection of *C* and *M* pixels is proposed as well.

5. Results and discussion

The procedure to define the position of *C* and *M* pixels, crucial for applying the procedure, mostly in ungauged sites was firstly analysed. Then, the correlation between *Q* and *v* time series and the C/M^* ratio was evaluated. Finally, a regional relationship between satellite and *in-situ* time-series was investigated in order to validate MODIS data also for ungauged river sites. For this last purpose, the C/M^* agreement with *in situ* data was also investigated by randomly selecting the *C* and *M* pixels.

Fig. 4. Maps of the maximum coefficient of correlation, *r*, between C/M^* and *v* time series obtained varying the location of pixel *C* and fixing *M* in each pixel (first column) and viceversa (second column). The location of the *C* and *M* pixels having the absolute maximum correlation is shown. The optical satellite image corresponding to the selected box taken from Google Earth™ is shown in the third column. Rows correspond to: (a,b,c) Piacenza, (d,e,f) Cremona, (g,h,i) Borgoforte, and (l,m,n) Pontelagoscuro gauging stations.

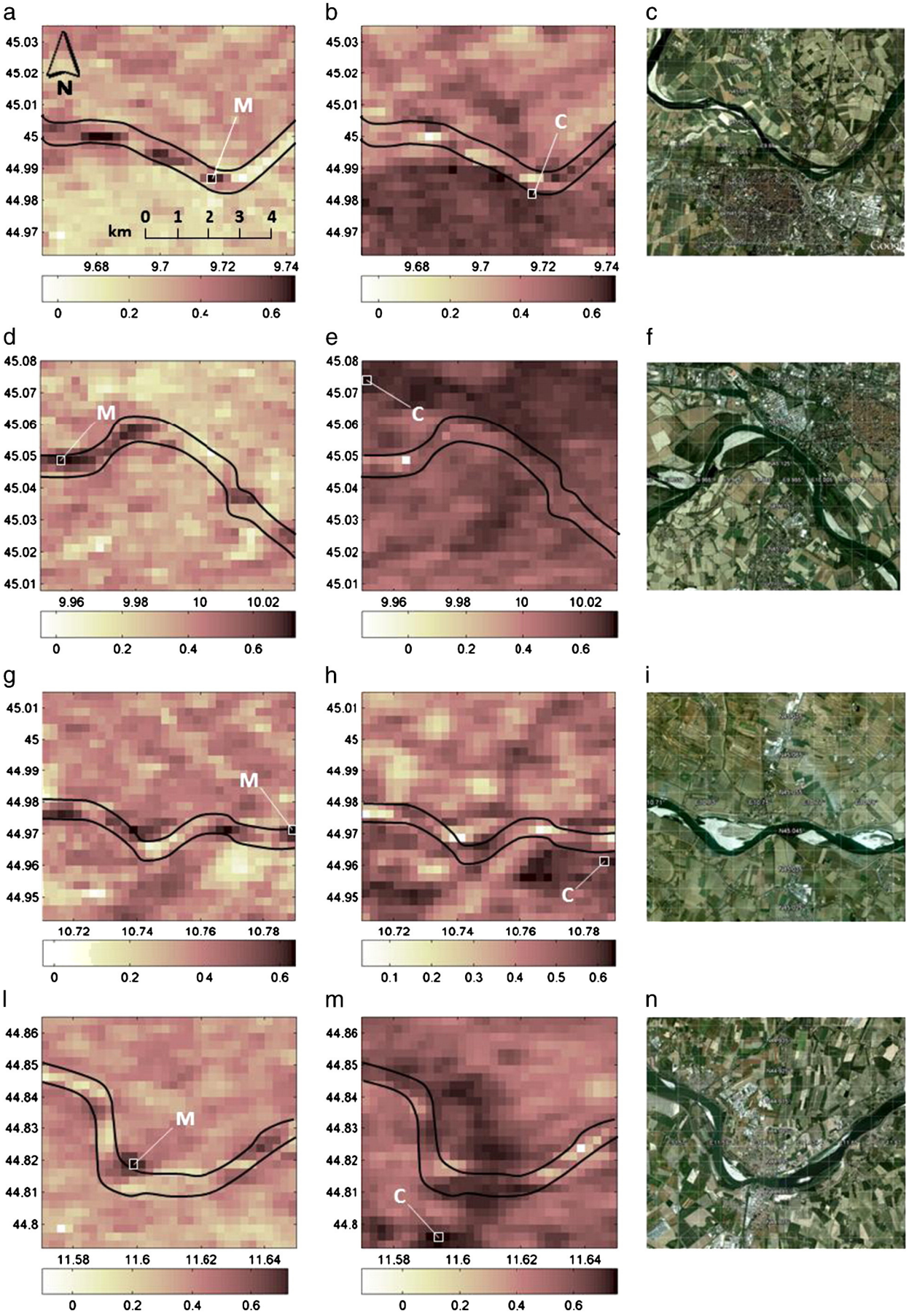

5.1. Selection of the M and C pixel location

For each site a box of 28 × 32 (=896) pixels centered on the investigated gauging stations was selected. Firstly, all the pixels with a value of channel's 1 reflectance higher than 0.2 were excluded. However, this procedure was found to be not sufficient as shown in Fig. 3. In fact, for cloud-free images the detection of the river, with very low reflectance values, is easily identifiable (Fig. 3a) while this is not true for images affected by clouds and/or residual fog, which are very common in the investigated areas (Fig. 3b). To avoid this problem, each single image was visually checked to be sure of analysing only cloud/fog-free images; in Table 2 the number of images selected for each site is reported. By considering that the total number of available Aqua-MODIS images is equal to 2832 the percentage of selected images is always lower than 50%. However, as a seven-year time period was analysed, the employed data set can be assumed as highly robust for evaluating the reliability of MODIS data in the estimation of discharge.

To identify the best locations for the *C* and *M* pixels the *C*/*M* ratio was calculated for each pixel of each box surrounding the gauging station thus obtaining [28 × 32] × [28 × 32 − 1] time series of *C*/*M* ratios. More specifically, each single pixel of the box was assumed to be *M* and, considering the remaining pixels (28 × 32 − 1) as *C*, 895 *C*/*M* time series were calculated in the selected pixel. The procedure was repeated for all the pixels of the box (896). In addition, different *T* values of the exponential smoothing filter in the range $T = 1 \div 20$ days were used, in order to take the satellite revisit time (16 days) into account. As a result, at each pixel 895 × 20 C/M^* time series were obtained and each one was compared with the *in situ* observed flow velocity time series.

For all the four sites, the maximum correlation *r*-values, between satellite and observed time series were found with a *T*-value nearly equal to 10 days. This value for *T* allows us to minimize the errors due to different illumination conditions as it can be expected considering the repeating 16-day orbit cycle of the MODIS sensor. Therefore, the maximum coefficients of correlation *r* between C/M^* and *v* time series, varying the *C* location, were obtained (for a total of 896) by using all available dates (see Table 2) and extracting the maximum for each pixel. They are represented in the first column of Fig. 4 (Fig. 4a, d, g, l) where the best location for the *M* pixel can be identified. As expected, the highest *r*-values are located along the water course whereas the lowest are far from it.

In order to identify the *C* pixel location, the above procedure was repeated assuming each pixel of the box as *C* and varying the *M* pixel to maximize the correlation between C/M^* and v time series. The maximum coefficients of correlation r for each pixel were obtained and shown in the second column of Fig. 4 (Fig. 4b, e, h, m). In this case the lowest r-values are located along the water course (light pixels). In the third column of Fig. 4 (Fig. 4c, f, i, n), the optical satellite image corresponding to the selected box and taken from Google Earth™ is shown to investigate the relationship between the location of the *C* and *M* pixels and the land use and river morphology characteristics of the area. As it can be seen, from Fig. 4a–c it is possible to note that the maximum correlation occurs when *M* is located in correspondence with the meanders, for which higher sensitivity to water variability is expected. On the other hand, for the pixel *C* the higher *r*-values are located in correspondence with urban areas (see Fig. 4b). For these areas a nearly constant reflectance was observed (not affected by the seasonal variability of vegetation), and hence, they are the best candidates for the location of *C* pixels. To extend the results to regions in which urban areas are not present, the temporal coefficient of variation of the reflectance of each pixel was computed. By comparing these maps (see Fig. 5) with the second column

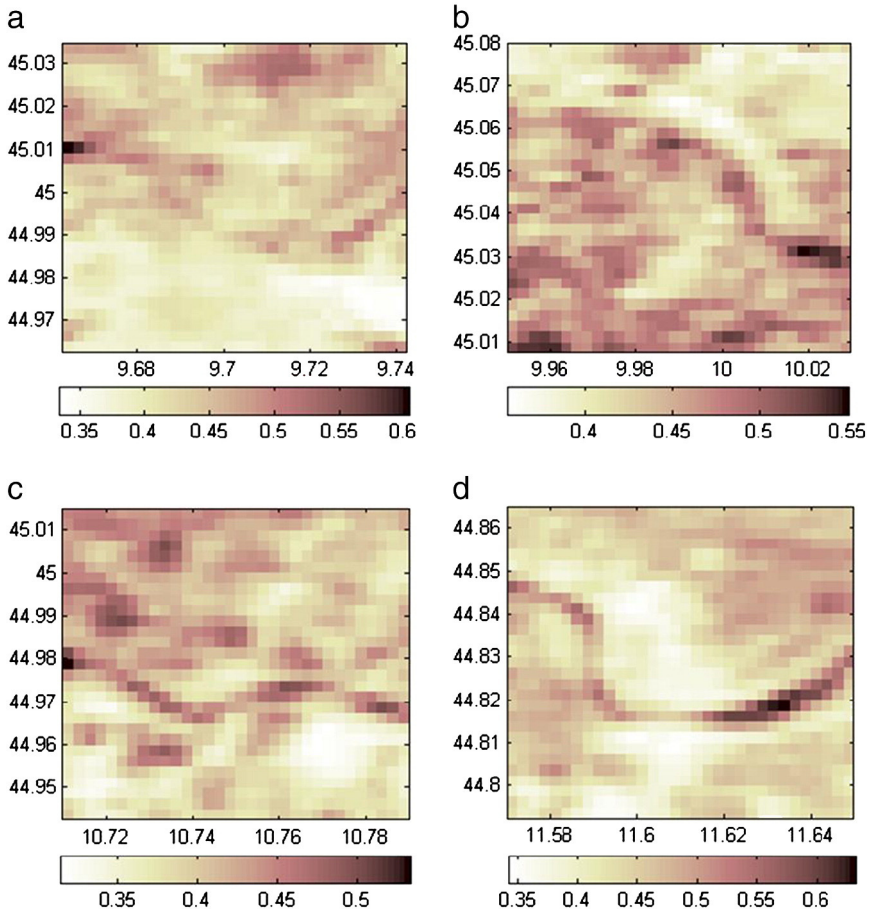

Fig. 5. Maps of temporal coefficients of variation of the reflectance values for the four investigated sites: a) Piacenza, b) Cremona, c) Borgoforte and d) Pontelagoscuro.

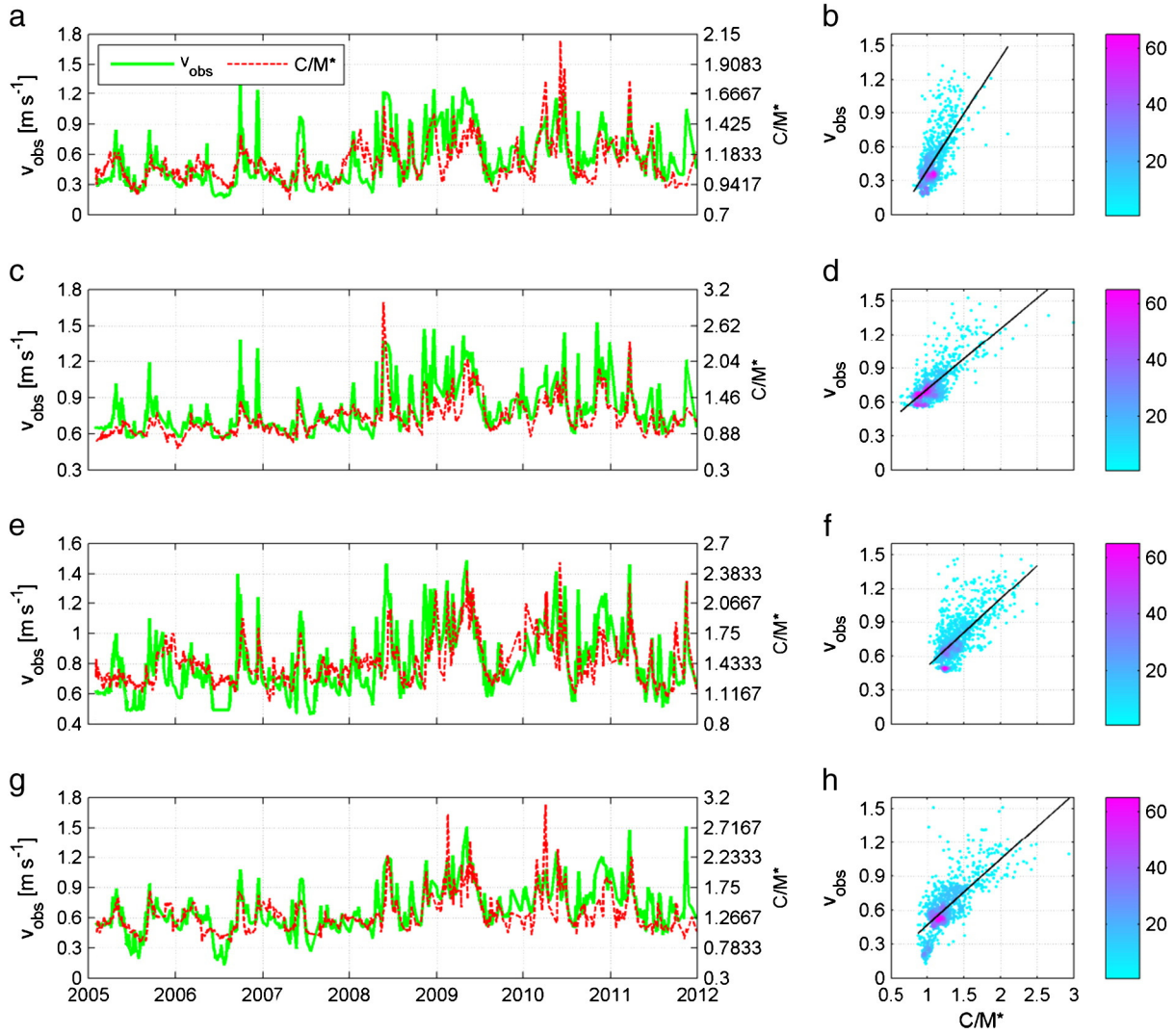

Fig. 6. Temporal pattern (left) and scatter plot (right) of 'observed' mean flow velocity, v_{obs}, versus the filtered C/M time series, C/M^*, for the four investigated sites: a,b) Piacenza, c,d) Cremona, e,f) Borgoforte and g,h) Pontelagoscuro.

of Fig. 4, it was found that the best areas for the location of the C pixels correspond to those with lowest coefficients of variation. Specifically, by comparing the two maps, pixels showing a temporal variability less than 0.4 can be selected to identify the C location. Similar findings are also obtained for all the gauging stations (see Fig. 4) thus confirming the robustness of this rule.

5.2. Correlation between in situ and satellite data

Once the position of M and C was selected maximizing the coefficient of correlation between C/M^* and v time series (by using all the available dates, see Fig. 4), the same pixels were also employed for the comparison with Q; all the results are summarized in Table 2. As it

Table 3
Performance of the relationship between 'observed' mean flow velocity and the C/M^* ratio, in terms of root mean square error, *RMSE*, and Nash–Sutcliffe efficiency, *NS* for the velocity, v, and discharge, Q.

Gauged station	*In situ* relationship						Regional relationship					
	RMSE	NS	MAE	Percentile			RMSE	NS	MAE	Percentile		
				10th	50th	90th				10th	50th	90th
$C/M^* - v$												
Piacenza	0.17	0.45	0.13	0.02	0.10	0.26	0.21	0.20	0.18	0.04	0.18	0.31
Cremona	0.11	0.59	0.08	0.01	0.06	0.17	0.22	−0.46	0.18	0.05	0.17	0.32
Borgoforte	0.15	0.46	0.11	0.01	0.08	0.22	0.15	0.46	0.11	0.01	0.08	0.22
Pontelagoscuro	0.16	0.55	0.12	0.02	0.09	0.24	0.16	0.49	0.13	0.02	0.10	0.27
$C/M^* - Q$												
Piacenza	273	0.65	181	27	131	369	297	0.59	238	47	228	388
Cremona	192	0.89	102	10	57	205	324	0.68	225	46	169	454
Borgoforte	268	0.83	154	14	102	332	265	0.83	155	16	103	326
Pontelagoscuro	312	0.78	197	28	138	388	298	0.80	206	30	164	360

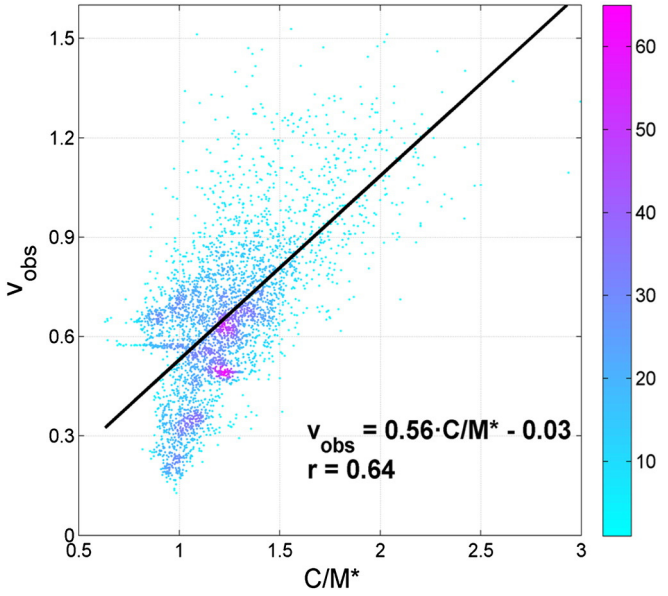

Fig. 7. Regional relationships between the filtered C/M^* ratio and the mean flow velocity, v_{obs}, for Po river.

can be seen, the unfiltered C/M ratio is found to be poorly correlated with both Q and v, with r-values in the range 0.48–0.61, and it can be attributed to the noise of the signal due to atmospheric contribution and illumination conditions. On the other hand, if exponential smoothing filter is applied, the r-values significantly increase, confirming the potential of this approach to reduce the impact of random errors on long time series. The correlation r for the velocity is slightly higher than for the discharge with values ranging from 0.67 to 0.77 for Piacenza and Cremona gauging stations, respectively.

Fig. 6 shows the comparison between the C/M^* and the v time series, normalized to identify approximately the same range of variability, for all the gauging stations. The C/M^* index closely follows the seasonal pattern of v with higher values in the winter season and lower in summer. Interestingly, MODIS-derived data are also able to identify the difference in the v values among the different years. In fact, in 2006 and 2007 the C/M^* values were considerably lower than in 2009 and 2010 in good accordance with the *in situ* observations for all gauging stations. Nonetheless, there are some significant discrepancies; for instance, on Fig. 6e, in the middle of the years 2006 and 2007 the measured v has two considerable 'lows' while the C/M^* show two highs. These differences must be attributed to the residual noise not accounted for in the developed procedure (computation of the C/M ratio and exponential filtering), but they are mainly due to the different nature of the two time series.

A linear regression was computed between C/M^* and v time series and the results are shown in the Fig. 6b, d, f and h. The performance of the linear regression is quite satisfactory with RMSE-values lower than 0.17 ms^{-1}, NS in the range 0.45–0.59 and MAE lower than 0.13 ms^{-1} (see Table 3). If the results are expressed in terms of discharge, Q, computed as the products between flow velocity and area, even better findings are achieved. In this case, *RMSE* values are lower than 320 m^3s^{-1}, *NS* is higher than 0.65 with a maximum equal to 0.89 for Cremona station and MAE in the range 102–197 m^3s^{-1} (Table 3). The analysis of the absolute error distribution for each gauging station showed that the median values (50th percentile) are lower than the mean (MAE) for both Q and v. Moreover, in 90% of cases, the error is lower than 0.26 ms^{-1} (the maximum absolute error is 1 ms^{-1}) for the velocity and lower than 390 m^3s^{-1} for the discharge confirming the robustness of the results. The obtained results are noteworthy also because they are significantly better than those obtained for two of the gauging stations (Piacenza and Pontelagoscuro) by applying the same approach to AMSR-E data (http://old.gdacs.org/flooddetection/overview.aspx). In fact, the correlation between the discharge time series extracted by the Global Flood Detection System and *in situ* observation at Piacenza and Pontelagoscuro are found to be equal to 0.35 and 0.58, respectively (Tarpanelli et al., 2012). This discrepancy is likely to be related to the coarser spatial resolution of AMSR-E measurements (~15 km at 37 GHz) and this confirms the potential of MODIS data for improving discharge estimation particularly over medium-sized basins (<10,000 km^2).

5.3. Application to ungauged sites in the Po basin

The satellite and *in-situ* time-series of all the four gauging stations were further analysed in order to find a single regional relationship to be applied to ungauged sites (see Fig. 7). In Table 3 the performance for the regional relationship is reported. As expected, all the performances have worsened. In particular, slightly lower *NS*-values were obtained but still satisfactory when discharge is considered (NS = 0.59–0.83). The regional relationship affected negatively mostly in the Cremona station, where the highest errors were calculated. In principle, this relationship, being quite robust and valid for two stations (Piacenza and Pontelagoscuro) separated by a long distance (236 km), can also be used for estimating discharge to the ungauged site of the Po river.

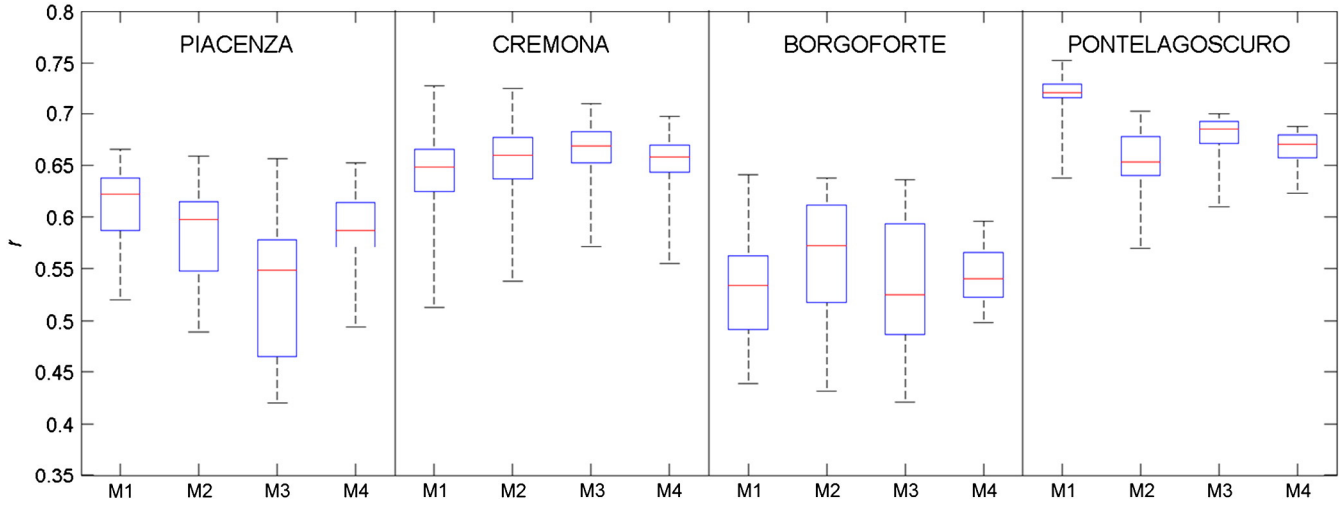

Fig. 8. Boxplot with whiskers from minimum to maximum of the coefficient of correlation, r, between the velocity, v and the C/M^* ratio calculated for the four best M pixels (M1–M4) and different locations of C pixels randomly selected in the urban areas.

For application of the procedure to ungauged sites, the second issue is the identification of the location for the *C* and *M* pixels. In this paragraph, taking account of the guidelines given above, the effect of randomly selecting the location of *C* and *M* pixels is assessed.

For this purpose, the best four pixels for the *M* position were selected (i.e., showing the higher correlations with *v* time series) and the location of *C* pixels was randomly sampled within the urban area. From their combination different coefficients of correlation were obtained that are represented in the box plot of Fig. 8. The performance still remains in a range with *r*-values always greater than 0.4. In particular, the best performance is observed for the Pontelagoscuro box, in which the average *r*-values remain above 0.65. With this preliminary analysis is intended to apply the procedure also for ungauged river sites even though further tests in different contexts are needed to assess its reliability.

6. Conclusions

An analysis for the evaluation of the capability of MODIS channel 1 and 2 data to estimate river discharge along the Po river (North Italy) was carried out. For this purpose, the approach proposed by Brakenridge et al. (2005), based on the computation of the *C*/*M* ratio of channel 2 reflectance values between a "water" (*M*: measurement) and a "land" (*C*: calibration) pixel, was used by considering seven years of Aqua MODIS data (2005-2011). Results show that, after the application of a smoothing filter to reduce noise, the C/M^* time series are in good agreement with both the discharge and mean flow velocity time series measured at four specific gauging stations within the investigated area. In particular, significant correlation values, *r*, are obtained and equal to, on average, 0.72 and 0.70 for the mean flow velocity and discharge, respectively (Fig. 5). Moreover, a regional relationship between C/M^* and velocity, *v*, time series is also derived (Fig. 6) showing $r = 0.64$ and low estimation errors (Table 3). Additionally, the best location for *C* and *M* pixels was found to be in urban areas (with a nearly constant temporal behaviour of channel 2 reflectance values) and near the meanders, respectively. The regional relationship and these guidelines for locating *C* and *M* pixels can be used for estimating discharge in ungauged sites even though other rivers should be used to validate the real potential of the technique presented here, above all for poorly gauged regions.

Overall, this study has shown that MODIS data can give good estimates of discharge for medium sized basins (<10,000 km^2) characterized by high temporal variability and can be used also for ungauged river sites. The capability of MODIS to estimate mean flow velocity could be efficiently employed for rating curve development at ungauged river sites by using simplified routing approaches (Moramarco et al., 2005; Perumal et al., 2007), and this is will be the object of future investigations. Moreover, MODIS data can also be used together with other satellite sensors (SAR, altimeter), to constrain hydrologic/hydraulic modelling simulations allowing for a reduction in their predictive uncertainty.

Acknowledgments

The authors wish to thank R. Rosi for his technical assistance, ARPA (Agenzia Regionale Prevenzione e Ambiente) Emilia Romagna and in particular, Eng. Federica Pellegrini, for providing the analysed data for Po River basin.

References

IAHS Ad Hoc Committee (2001). Global water data: A newly endangered species. *Eos, Transactions of the American Geophysical Union*, *82*(5), 54.

Albergel, C., Rüdiger, C., Pellarin, T., Calvet, J. C., Fritz, N., Froissard, F., et al. (2008). From near-surface to root-zone soil moisture using an exponential filter: An assessment of the method based on *in-situ* observations and model simulations. *Hydrology and Earth System Sciences*, *12*, 1323–1337. http://dx.doi.org/10.5194/hess-12-1323-2008.

Alsdorf, D. E., Rodriguez, E., & Lettenmaier, D. P. (2007). Measuring surface water from space. *Review of Geophysics*, *45*, RG2002. http://dx.doi.org/10.1029/2006RG000197.

Birkinshaw, S. J., O'Donnell, G. M., Moore, P., Kilsby, C. G., Fowler, H. J., & Berry, P. A. M. (2010). Using satellite altimetry data to augment flow estimation techniques on the Mekong River. *Hydrological Processes*, *24*, 3811–3825.

Bjerklie, D. M., Dingman, S. L., Vorosmarty, C. J., Bolster, C. H., & Congalton, R. G. (2003). Evaluating the potential for measuring river discharge from space. *Journal of Hydrology*, *278*, 17–38.

Brakenridge, G. R., & Anderson, E. (2006). MODIS-based flood detection, mapping and measurement: the potential for operational hydrological applications. In J. Marsalek, G. Stancalie, & G. Balint (Eds.), *Proceedings of the NATO on Transboundary floods: reducing risk through flood management*, *Vol. 72*. (pp. 1–12).

Brakenridge, G. R., Cohen, S., Kettner, A. J., De Groeve, T., Nghiem, S. V., Syvitski, J. P. M., & Fekete, B. M. (2012). Calibration of satellite measurements of river discharge using a global hydrology model. *Journal of Hydrology*, *475*, 123–136. http://dx.doi.org/10.1016/j.jhydrol.2012.09.035.

Brakenridge, G. R., Nghiem, S. V., Anderson, E., & Chien, S. (2005). Space-based measurement of river runoff. *Eos, Transactions of the American Geophysical Union*, *86*(19), 185–192.

Brakenridge, G. R., Nghiem, S. V., Anderson, E., & Mic, R. (2007). Orbital microwave measurement of river discharge and ice status. *Water Resources Research*, *43*, W04405.

Calmant, S., & Seyler, F. (2006). Continental surface water from satellite altimetry. *Comptes Rendus Geosciences*, *338*(14–15), 1113–1122. http://dx.doi.org/10.1016/j.crte.2006.05.012.

De Groeve, T., & Riva, P. (2009). Early flood detection and mapping for humanitarian response. *Proceedings of the 6th International ISCRAM Conference — Gothenburg, Sweden*.

Di Baldassarre, G., & Uhlenbrook, S. (2011). Is the current flood of data enough? A treatise on research needs for the improvement of flood modelling. *Hydrological Processes*. http://dx.doi.org/10.1002/hyp.8226.

Faruolo, M., Coviello, I., Lacava, T., Pergola, N., & Tramutoli, V. (2009). Real Time Monitoring of flooded areas by a multi-temporal analysis of optical satellite data. *Proc. IEEE International Geoscience and Remote Sensing Symposium*, *4*. (pp. 192–195).

Friedl, M. A., Sulla-Menashe, D., Tan, B., Schneider, A., Ramankutty, N., Sibley, A., et al. (2010). MODIS Collection 5 global land cover: Algorithm refinements and characterization of new datasets. *Remote Sensing of Environment*, *114*, 168–182.

Horritt, M. S., Mason, D. C., & Luckman, A. J. (2001). Flood boundary delineation from synthetic aperture radar imagery using a statistical active contour model. *International Journal of Remote Sensing*, *22*, 2489–2507.

Matgen, P., Hostache, R., Schumann, G., Pfister, L., Hoffmann, L., & Savenije, H. H. G. (2011). Towards an automated SAR-based flood monitoring system, lessons learned from two case studies. *Physics and Chemistry of the Earth*, *36*, 241–252.

Moramarco, T., Barbetta, S., Melone, F., & Singh, V. P. (2005). Relating local stage and remote discharge with significant lateral inflow. *Journal of Hydrologic Engineering*, *10*, 58–69.

Nash, J. E., & Sutcliffe, J. V. (1970). River flow forecasting through conceptual models, Part I: A discussion of principles. *Journal of Hydrology*, *10*(3), 282–290.

Neal, J., Schumann, G., Bates, P., Buytaert, W., & Pappenberger, F. (2009). A data assimilation approach to discharge estimation from space. *Hydrological Processes*, *23*, 3641–3649.

Perumal, M., Moramarco, T., Sahoo, B., & Barbetta, S. (2007). A methodology for discharge estimation and rating curve development at ungauged river sites. *Water Resources Research*, *43*, W02412.

Smith, L. C., Isacks, B. L., Bloom, A. L., & Murray, A. B. (1996). Estimation of discharge from three braided rivers using synthetic aperture radar satellite imagery. *Water Resources Research*, *32*(7), 2021–2034.

Smith, L. C., & Pavelsky, T. M. (2008). Estimation of river discharge, propagation speed, and hydraulic geometry from space: Lena River, Siberia. *Water Resources Research*, *44*, W03427.

Tarpanelli, A., Brocca, L., Lacava, T., Faruolo, M., Melone, F., Moramarco, T., et al. (2012). Using MODIS data to estimate river discharge in ungauged sites. *Geophysical Research Abstracts*, *14*, EGU2012–EGU3132.

Tarpanelli, A., Brocca, L., Melone, F., Moramarco, T., Lacava, T., Faruolo, M., et al. (2011). River discharge estimation through MODIS data. In C. M. U. Neale, A. Maltese, & K. Richter (Eds.), *Remote Sensing for Agriculture, Ecosystems, and Hydrology, XIII. Proc. of SPIE*, *Vol. 8174*. (pp. 817408). http://dx.doi.org/10.1117/12.898201 (8 pp.).

Temimi, M., Leconte, R., Brissette, F., & Chaouch, N. (2007). Flood and soil wetness monitoring over the Mackenzie River Basin using AMSR-E 37 GHz brightness temperature. *Journal of Hydrology*, *333*, 317–328.

Temimi, M., Romanov, P., Ghedira, H., Khanbilvardi, R., & Smith, K. (2011). Sea ice monitoring over the Caspian Sea using geostationary satellite data. *International Journal of Remote Sensing*, *32*(6).

Wagner, W., Lemoine, G., & Rott, H. (1999). A method for estimating soil moisture from ERS scatterometer and soil data. *Remote Sensing of Environment*, *70*, 191–207.

Weissling, B. P., & Xie, H. (2008). Proximal watershed validation of a remote sensing-based streamflow estimation model. *Journal of Applied Remote Sensing*, *2*, 023549. http://dx.doi.org/10.1117/1.3043664.

Weissling, B. P., & Xie, H. (2009). MODIS biophysical states and NEXRAD precipitation in a statistical evaluation of antecedent moisture condition and streamflow. *Journal of the American Water Resources Association*, *45*, 419–433.